

Theory of quantum fluctuations of optical dissipative structures and its application to the squeezing properties of bright cavity solitons

Isabel Pérez-Arjona⁽¹⁾, Eugenio Roldán⁽²⁾, and Germán J. de Valcárcel⁽²⁾

⁽¹⁾*Departament de Física Aplicada, Escola Politècnica Superior de Gandia, Universitat Politècnica de València, Ctra. Natzaret-Oliva s/n, Spain and*

⁽²⁾*Departament d'Òptica, Universitat de València, Dr. Moliner 50, 46100-Burjassot, Spain*

We present a method for the study of quantum fluctuations of dissipative structures forming in nonlinear optical cavities, which we illustrate in the case of a degenerate, type I optical parametric oscillator. The method consists in (i) taking into account explicitly, through a collective variable description, the drift of the dissipative structure caused by the quantum noise, and (ii) expanding the remaining -internal- fluctuations in the biorthonormal basis associated to the linear operator governing the evolution of fluctuations in the linearized Langevin equations. We obtain general expressions for the squeezing and intensity fluctuations spectra. Then we theoretically study the squeezing properties of a special dissipative structure, namely, the bright cavity soliton. After reviewing our previous result that in the linear approximation there is a perfectly squeezed mode irrespectively of the values of the system parameters, we consider squeezing at the bifurcation points, and the squeezing detection with a plane-wave local oscillator field, taking also into account the effect of the detector size on the level of detectable squeezing.

PACS numbers: 42.50.L; 42.65.Sf

I. INTRODUCTION

Quantum fluctuations in the light field observables have been a subject of intensive and maintained research since the appearance of quantum optics in the early sixties, especially since the discovery of the nonclassical states of light and the generation of squeezed light in the mid eighties [1]. Quantum fluctuations are unavoidable as their origin lies in the impossibility of determining two canonically conjugate observables with a precision better than that allowed by the Heisenberg uncertainty relations. In the case of the radiation field, quantum fluctuations manifest in quantities such as the photon number, the field phase, the Stokes parameters, or the field quadratures [2, 3, 4, 5, 6].

Although its origin could be traced back till the early days of quantum mechanics [5], the modern squeezing research goes back to the mid seventies, its foundational period being closed with the experimental generation of squeezed light in the mid eighties [3]. In a single-mode state the two field quadratures (equivalent to the position and momentum operators of a harmonic oscillator) constitute a canonically conjugate pair, the product of their uncertainties being consequently limited by the Heisenberg inequality. When the field mode is in a coherent state, the uncertainty is the same for any field quadrature and equals that of the vacuum state. Then, a squeezed state is that for which the uncertainty in a particular field quadrature is smaller than that of the quantum vacuum, a reduction achieved at the expense of an increase in the uncertainty of the complementary field quadrature. These states can be generated in nonlinear processes (four-wave mixing, parametric down-conversion...), and the field quadratures can be detected in a homodyne detection experiment in which the quantum state is mixed with a classical (intense, coherent) local oscillator field

[2].

Single-mode squeezing has been intensively and extensively investigated for almost three decades [1]. A well established result is that a high degree of squeezing is obtained in nonlinear cavities near the bifurcation points, and that the squeezing level degrades as the system is brought far from them [6]. Multimode squeezing has also been considered in the past. One of the most immediate cases is that of nonlinear cavities working in several longitudinal modes, a type of system already exhibiting noise reduction features specific to multimode systems. For example, the quantum noise suppression on the difference of intensities (amplitude-squeezing) of a two-mode optical parametric oscillator above threshold [7, 8], which is associated to the existence of a continuous diffusion of the phase difference between the two modes. It is to be remarked that squeezing appears in this case associated to a *collective variable*, namely the intensity difference, and that, remarkably, the noise reduction level is independent of the system proximity to a bifurcation point.

A particularly interesting case of multimode squeezing is that of solitons. Squeezing in optical fibre solitons (*temporal* solitons) has attracted much interest since the late eighties [9, 10] and is by now quite well understood, see e.g. [11] for a recent review. In this problem the relevance of collective variables, such as the position or the momentum of the soliton, is very clear in the sense that these are the observables in which the behavior of quantum fluctuations is easily detectable. As we comment below, this problem has some similarities, but also strong differences, with the problem of cavity solitons that we treat here. A related problem, that of the squeezing of spatial solitons in Kerr media, has also been considered recently [12, 13, 14, 15].

For our purposes, a most exciting connection is that existing between pattern formation in nonlinear optical

cavities and squeezing [16, 17]. In these systems the concepts used in the analysis of quantum fluctuations, which has started relatively recently, must be generalized to cover correlations at different spatial points [18].

Extended nonlinear optical systems, specially nonlinear optical cavities with large Fresnel numbers, are systems that spontaneously display dissipative structures, which are extended patterns that form in the plane orthogonal to the light propagation direction, through an spontaneous symmetry breaking. One of the new concepts that appeared when the analysis of quantum fluctuations in these systems was addressed is the quantum image [19], which can be described as a precursor appearing below threshold of the pattern that the system would display above threshold. The quantum image is not detectable at low observation frequencies as in this case the fast dynamics of quantum fluctuations is washed out. We refer the reader to existing reviews for a resume of the main researches in the field [16, 17]. For our purposes, which concern the analysis of the squeezing in dissipative structures, the work carried out by Gatti and Lugiato [20, 21] on the squeezing of extended degenerate optical parametric oscillators (DOPO) below threshold, is particularly close (see also [22]), as well as the analysis of the role played by the Goldstone mode in [23, 24].

In this article we investigate quantum fluctuations of dissipative structures in the DOPO. In a first part we develop the theory for the calculation of linearized quantum fluctuations, in particular for the calculation of the squeezing and intensity fluctuations spectra. The theory is general in the sense that no particular dissipative structure is assumed. Moreover, although the model for a DOPO in the large pump detuning is used, the derived expressions are easily generalizable to cover other nonlinear cavity models. Then, in a second part we apply this theory to the study of the squeezing properties of a special dissipative structure appearing above threshold, the so-called bright cavity soliton.

In [25] we already advanced a particular property of quantum fluctuations which is specific to pattern formation (i.e., that is absent when the emission is homogeneous in space), which can be put in short as follows: Due to the translational invariance of the problem (the position of the pattern in the transverse plane is not fixed when the pumping is spatially homogeneous), there is a particular transverse mode that is free from quantum fluctuations (in the linear approximation), a *perfectly* squeezed mode. And this occurs irrespectively of the value of the parameters of the system. The only conditions are that (i) the system be translational invariant, and (ii) that the output field displays a pattern. This particular mode corresponds to the transverse linear momentum of the pattern.

Here we shall go beyond this result by studying the squeezing properties of a special pattern, the bright cavity soliton. For that we shall consider the DOPO model in the large pump detuning limit, as the problem is much simpler in these conditions because there exists an ex-

plicit analytical solution for the localized structure. As stated, the article consists of two parts. In the first part (covering Sections II to V) we derive general expressions for the study of quantum fluctuations (e.g., the linear squeezing spectrum) without specializing to any particular pattern. Then, the second part (Section VI) is devoted to the bright cavity soliton. Finally, in Section VII we give our main conclusions.

II. LINEAR THEORY OF QUANTUM FLUCTUATIONS OF OPTICAL DISSIPATIVE STRUCTURES

In this section we present the general method that will allow us determining quantities related with the quantum fluctuations of optical dissipative structures (e.g. the squeezing spectrum) in the linear approximation. An outstanding feature of the method is that it circumvents the numerical integration of the dynamical, stochastic equations, which is always a problematic (and terribly time consuming) task. Instead, the method exploits the diagonalization of the linear problem, which allows simple formal solutions.

We shall use the DOPO with plane cavity mirrors as a model for presenting the method. Any other nonlinear optical cavity with plane mirrors sustaining dissipative structures can be studied along similar ways after straightforward particularization of the expressions given below.

We assume that the dynamical equations of the studied system have been cast in the form of classical-looking Langevin equations corresponding to some coherent state representation. In particular we assume that a generalized P representation [27] is being used (Sec. II.A) as its normal ordering equivalence allows a direct computation of measurable quantities corresponding to the fields leaving the cavity. Furthermore we assume that those Langevin equations have been linearized around a classical dissipative structure (Sec. II.B). The method consists in separating the fluctuations in two classes: (i) Those coming from the drift of the dissipative structure, as it can move freely across the transverse section owed to the spatial translation invariance of the model (Sec. II.C); and (ii) Formally solving the equations corresponding to the remaining ("internal") fluctuations making use of a special basis (Sec. II.D), what allows deriving a general expression for the linearized squeezing spectrum (Sec. III), as well as for the spectrum of intensity fluctuations (Sec. IV). This section ends with a general result concerning the squeezing of dissipative structures (Sec. V).

A. Langevin equations for a planar DOPO in the generalized P representation

We consider the model for a type I DOPO with plane cavity mirrors of [26] pumped by a plane wave coherent

field of frequency $2\omega_s$ and amplitude \mathcal{E}_{in} . An intracavity $\chi^{(2)}$ nonlinear crystal converts pump photons into sub-harmonic photons, at frequency ω_s , and vice versa. Only two longitudinal cavity modes, of frequencies ω_0 (pump mode) and ω_1 (signal mode), which are the closest to $2\omega_s$ and ω_s , respectively, are assumed to be relevant. The cavity is assumed to be single-ended, i.e., losses occur at a single cavity mirror, where the intracavity modes are damped at rates γ_n , $n = 0, 1$. The above frequencies define dimensionless pump and signal detuning parameters through $\Delta_0 = (\omega_0 - 2\omega_s)/\gamma_0$ and $\Delta_1 = (\omega_1 - \omega_s)/\gamma_1$, respectively.

We denote the intracavity field envelope operators for pump and signal modes, which propagate along the z direction, by $\hat{A}_0(\mathbf{r}, t)$ and $\hat{A}_1(\mathbf{r}, t)$, respectively, where $\mathbf{r} = (x, y)$ is the transverse position vector, obeying standard equal-time commutation relations

$$[\hat{A}_m(\mathbf{r}, t), \hat{A}_n^\dagger(\mathbf{r}', t)] = \delta_{m,n} \delta(\mathbf{r} - \mathbf{r}'). \quad (1)$$

As commented we shall use a coherent state representation in order to handle the problem. These representations set a correspondence between the quantum operators $\hat{A}_m(\mathbf{r}, t)$ and $\hat{A}_m^\dagger(\mathbf{r}, t)$ and the c-number fields $\mathcal{A}_m(\mathbf{r}, t)$ and $\mathcal{A}_m^+(\mathbf{r}, t)$, respectively, which are independent but in their (stochastic) averages, which verify $\langle \mathcal{A}_m^+(\mathbf{r}, t) \rangle = \langle \mathcal{A}_m(\mathbf{r}, t) \rangle^*$. The physical meaning of the stochastic average of any function of the c-number fields depends on the representation. In particular we shall use the generalized P representation [27], generalized to include the spatial nature of the multimode problem here considered [26], in which the stochastic averages correspond to quantum expectation values computed in normal and time ordering.

As shown in Appendix A, in the large pump detuning limit ($|\Delta_0| \gg 1, |\Delta_1|, \gamma_0/\gamma_1$) the DOPO dynamical (Langevin) equations in the generalized P representation can be written as

$$\frac{\partial}{\partial t} \mathcal{A}_1(\mathbf{r}, t) = \gamma_1 \left(L_1 \mathcal{A}_1 + \mu \mathcal{A}_1^+ + i \frac{\sigma}{\kappa^2} \mathcal{A}_1^2 \mathcal{A}_1^+ \right) + \sqrt{\gamma_1 \left(\mu + i \frac{\sigma}{\kappa^2} \mathcal{A}_1^2 \right)} \eta(\mathbf{r}, t), \quad (2a)$$

$$\frac{\partial}{\partial t} \mathcal{A}_1^+(\mathbf{r}, t) = \gamma_1 \left(L_1^* \mathcal{A}_1^+ + \mu \mathcal{A}_1 - i \frac{\sigma}{\kappa^2} \mathcal{A}_1^{+2} \mathcal{A}_1 \right) + \sqrt{\gamma_1 \left(\mu - i \frac{\sigma}{\kappa^2} \mathcal{A}_1^{+2} \right)} \eta^+(\mathbf{r}, t), \quad (2b)$$

where $L_1 = -(1 + i\Delta_1) + il_1^2 \nabla^2$, $l_1 = c/\sqrt{2\omega_1\gamma_1}$ is the diffraction length for the signal field, $\nabla^2 = \partial^2/\partial x^2 + \partial^2/\partial y^2$ is the transverse Laplacian operator, and we have introduced the real and dimensionless parametric pump parameter μ

$$\mu = \frac{g|\mathcal{E}_{\text{in}}|}{\gamma_0\gamma_1|\Delta_0|} > 0, \quad (3)$$

where g is the (real) nonlinear coupling coefficient, Eq. (79) in Appendix A, the normalized nonlinear coupling coefficient

$$\kappa^{-2} = \frac{g^2}{2\gamma_0\gamma_1|\Delta_0|}, \quad (4)$$

and $\sigma = \text{sign } \Delta_0 = \pm 1$. Finally, $\eta(\mathbf{r}, t)$ and $\eta^+(\mathbf{r}, t)$ are independent, real white Gaussian noises of zero average and correlations given by Eqs. (85) in Appendix A.

Equations (2) are the model we shall consider along this paper.

B. Dynamics of quantum fluctuations: Linearized Langevin equations around the classical dissipative structures of the DOPO

In the classical limit (\mathcal{A}_i^+ being interpreted as \mathcal{A}_i^* , noises being ignored), Eqs. (87) have the form of a parametrically driven nonlinear Schrödinger equation (PDNLSE), first derived for the DOPO in [30, 31], see Eq. (88) in Appendix B. In our case σ accounts for the cases of self-focusing ($\sigma = +1$) or defocusing ($\sigma = -1$) of the PDNLSE, which determine the kind of dissipative structures (DS) supported by the DOPO. These DS are patterns that appear in the transverse plane with respect to the direction of light propagation. We denote these (steady) structures by $\bar{\mathcal{A}}_1(\mathbf{r}) = \bar{\mathcal{A}}_1(\mathbf{r} - \mathbf{r}_1)$, where $\mathbf{r}_1 = (x_1, y_1)$ is arbitrary due to the translation invariance of the problem. They can be, e. g., periodic patterns or localized structures [30, 32, 33, 34, 35]. Although in the second part of this paper we shall concentrate on a particular type of DS, namely the bright cavity soliton, we stress here that the treatment we present below is completely general and covers the description of quantum fluctuations of any stationary DS.

The dynamics of the quantum fluctuations around any DS is studied by setting

$$\mathcal{A}_1(\mathbf{r}, t) = \bar{\mathcal{A}}_1(\mathbf{r} - \mathbf{r}_1(t), t) + a_1(\mathbf{r} - \mathbf{r}_1(t), t), \quad (5a)$$

$$\mathcal{A}_1^+(\mathbf{r}, t) = \bar{\mathcal{A}}_1^*(\mathbf{r} - \mathbf{r}_1(t), t) + a_1^+(\mathbf{r} - \mathbf{r}_1(t), t), \quad (5b)$$

where $\bar{\mathcal{A}}_1$ and $\bar{\mathcal{A}}_1^*$ are the classical stationary mean values of the field corresponding to a particular DS (i.e., the stationary solutions of Eqs. (2) when the noise terms are neglected), and a_1 and a_1^+ are the c-number fields accounting for the quantum fluctuations. Notice that the position of the classical solution, $\mathbf{r}_1(t) = (x_1, y_1)$, is let to vary in time in order to properly describe the diffusive movement of the DS, which is excited by (quantum) noise.

Linearizing the Langevin equations around the classical solution we get, to first order in the fluctuations, the linearized equation of motion for the quantum fluctuations, that read

$$-\kappa \left(\mathbf{G}_x \frac{dx_1}{dt} + \mathbf{G}_y \frac{dy_1}{dt} \right) + \frac{\partial}{\partial t} \mathbf{a}_1 = \gamma_1 \mathcal{L} \mathbf{a}_1 + \sqrt{\gamma_1} \mathbf{h}, \quad (6)$$

where

$$\mathbf{G}_{x(y)} = \partial_{x(y)} \begin{pmatrix} \bar{\mathcal{A}}_1 \\ \bar{\mathcal{A}}_1^* \end{pmatrix}, \quad (7)$$

\mathbf{a}_1 is the quantum fluctuations vector

$$\mathbf{a}_1(\mathbf{r}, t) = \begin{pmatrix} a_1(\mathbf{r}, t) \\ a_1^+(\mathbf{r}, t) \end{pmatrix}, \quad (8)$$

\mathbf{h} is the noise vector

$$\mathbf{h}(\mathbf{r}, t) = \begin{pmatrix} \sqrt{\bar{\alpha}_0} \eta(\mathbf{r}, t) \\ \sqrt{\bar{\alpha}_0^*} \eta^+(\mathbf{r}, t) \end{pmatrix}, \quad (9)$$

where

$$\bar{\alpha}_0 = \mu + i\sigma\kappa^{-2}\bar{\mathcal{A}}_1^2. \quad (10)$$

Finally, the linear operator \mathcal{L} and its adjoint \mathcal{L}^\dagger read

$$\mathcal{L} = \begin{pmatrix} \mathcal{L}_1 & \bar{\alpha}_0 \\ \bar{\alpha}_0^* & \mathcal{L}_1^* \end{pmatrix}, \quad \mathcal{L}^\dagger = \begin{pmatrix} \mathcal{L}_1^* & \bar{\alpha}_0 \\ \bar{\alpha}_0^* & \mathcal{L}_1 \end{pmatrix}, \quad (11a)$$

$$\mathcal{L}_1 = -(1 + i\Delta_1) + i\bar{l}_1^2 \nabla^2 + 2i\sigma\kappa^{-2} |\bar{\mathcal{A}}_1(\mathbf{r})|^2, \quad (11b)$$

where we note that a typo has been corrected in Eq. (11b) with respect to the corresponding expression in [25].

In Eq. (6) two terms ($\partial_x \mathbf{a}_1 dx_1/dt$ and $\partial_y \mathbf{a}_1 dy_1/dt$) have been neglected as they are of second order in the fluctuations. Notice finally that Eq. (6) has the standard form of a set of linearized Langevin equations but for the first term appearing on the left hand side, which describes possible displacements of the DS on the transverse plane.

All the information about quantum fluctuations in the linear approximation is contained in Eq. (6). Our goal is then finding an efficient method for solving it at the time that relevant information is extracted in a transparent way. This is accomplished by using the eigensystems of the linear operators

C. Diagonalization of the linear problem. The role of the Goldstone modes: Drift of the dissipative structure

Our main purpose in this work is to study the properties of quantum fluctuations around the semiclassical mean value corresponding to a DS. In this section we solve Eqs. (6), which will allow to characterize the quantum fluctuations, in particular through the squeezing spectrum. With this aim, we develop a general method suitable for obtaining the formal solution of Eqs. (6), suitable for any system and any classical stationary DS.

Let us assume without proof that the set of eigenvectors of the linear operators \mathcal{L} and \mathcal{L}^\dagger , Eq. (11), form a biorthonormal basis. (In the second part of this article we show that this is indeed the case for the bright cavity soliton solution, unlike the problem of conservative temporal solitons where the set of eigenvectors must

be completed in order to form a proper basis [11]). The method used to solve Eq. (6) consists in expanding the quantum fluctuations in this biorthonormal basis.

We denote the eigensystems of \mathcal{L} and \mathcal{L}^\dagger by

$$\mathcal{L}\mathbf{v}_i(\mathbf{r}) = \lambda_i \mathbf{v}_i(\mathbf{r}), \quad \mathbf{v}_i(\mathbf{r}) = \begin{pmatrix} v_i(\mathbf{r}) \\ v_i^+(\mathbf{r}) \end{pmatrix}, \quad (12a)$$

$$\mathcal{L}^\dagger \mathbf{w}_i(\mathbf{r}) = \lambda_i^* \mathbf{w}_i(\mathbf{r}), \quad \mathbf{w}_i(\mathbf{r}) = \begin{pmatrix} w_i(\mathbf{r}) \\ w_i^+(\mathbf{r}) \end{pmatrix}. \quad (12b)$$

In the above and in the following expressions, the index i represents both the discrete and the continuous spectra as we do not want to overburden the notation. Note also that, in the following, Kronecker deltas should be understood as suitable Dirac deltas as well as sums should be understood as suitable integrals when referring to the continuous part of the spectra.

We define scalar product as usual

$$\langle \mathbf{u} | \mathbf{s} \rangle = \int d^2r \mathbf{u}^\dagger(\mathbf{r}) \cdot \mathbf{s}(\mathbf{r}), \quad (13)$$

so that relation

$$\langle \mathbf{w}_i | \mathcal{L} \mathbf{s} \rangle = \lambda_i \langle \mathbf{w}_i | \mathbf{s} \rangle, \quad (14)$$

holds for any \mathbf{s} . Finally, all eigenvectors are assumed to be normalized as

$$\langle \mathbf{w}_i | \mathbf{v}_j \rangle = \delta_{ij}. \quad (15)$$

The spectra must be computed numerically in general. However, it will be convenient for our purposes to state two general properties of the discrete spectra. These are:

- Property 1: For any parameter set there exist Goldstone modes, $\mathbf{v}_{1x(1y)} = \mathbf{G}_{x(y)}$, with $\mathbf{G}_{x(y)}$ given by Eq. (7), satisfying

$$\mathcal{L} \mathbf{v}_{1x(1y)} = 0, \quad (16)$$

and the associated adjoint eigenvectors, denoted by $\mathbf{w}_{1x(1y)}$, which verify

$$\mathcal{L}^\dagger \mathbf{w}_{1x(1y)} = 0. \quad (17)$$

This property is a consequence of the translational invariance of the problem, as any DS can be located at any position on the transverse plane.

- Property 2: For any parameter set there exist eigenvectors of the adjoint problem, which we denote as $\mathbf{w}_{2x(2y)}$, verifying

$$\mathcal{L}^\dagger \mathbf{w}_{2x(2y)} = -2\mathbf{w}_{2x(2y)}. \quad (18)$$

These eigenvectors are

$$\mathbf{w}_{2x(2y)}(\mathbf{r}) = \partial_{x(y)} \begin{pmatrix} i\bar{\mathcal{A}}_1(\mathbf{r}) \\ -i\bar{\mathcal{A}}_1^*(\mathbf{r}) \end{pmatrix}, \quad (19)$$

as is straightforward to be checked. This property will be associated to a perfectly squeezed mode [25], as we show below.

Now, the linearized Langevin equation (6) can be solved by expanding the quantum fluctuations on the basis $\{\mathbf{v}_i\}$,

$$\mathbf{a}_1(\mathbf{r}, t) = \sum_i c_i(t) \mathbf{v}_i(\mathbf{r}), \quad (20)$$

where the Goldstone modes have been excluded from this expansion as any contribution of them to $\mathbf{a}_1(\mathbf{r}, t)$ would entail a shift of the solution, which is already accounted for by the (still undetermined) location of the DS, by definition.

First we project Eq. (6) onto \mathbf{w}_{1x} and \mathbf{w}_{1y} , obtaining

$$\dot{x}_1 = -\frac{\sqrt{\gamma_1}}{\kappa} \langle \mathbf{w}_{1x} | \mathbf{h} \rangle, \quad (21a)$$

$$\dot{y}_1 = -\frac{\sqrt{\gamma_1}}{\kappa} \langle \mathbf{w}_{1y} | \mathbf{h} \rangle, \quad (21b)$$

We see that the DS diffuses driven by quantum fluctuations as anticipated. The diffusive drift of the DS through a time t_d can be evaluated by considering the mean squared deviation of the position of the DS along this time,

$$\boldsymbol{\rho}(t) = \mathbf{r}_1(t) - \mathbf{r}_1(t - t_d). \quad (22)$$

The variance $\langle \boldsymbol{\rho}^2(t) \rangle$ can be calculated from Eqs.(21), which give the time evolution for $\mathbf{r}_1 = (x_1, y_1)$, obtaining

$$x_1(t) = -\frac{\sqrt{\gamma_1}}{\kappa} \int_0^t dt' \langle \mathbf{w}_{1x}(\mathbf{r}) | \mathbf{h}(\mathbf{r}, t') \rangle, \quad (23)$$

and analogous expression holds for $y_1(t)$, when \mathbf{w}_{1x} is replaced by \mathbf{w}_{1y} in (23). Substituting this solution into Eq.(22), we reach the expression of the variance of $\boldsymbol{\rho}(t)$, which is linear in time [24], and reads

$$\langle \boldsymbol{\rho}^2(t) \rangle = Dt_d, \quad (24)$$

where the diffusion coefficient is given by

$$D = 2 \frac{\gamma_1}{\kappa^2} \text{Re} \int d^2r [w_{1x}^2(\mathbf{r}) + w_{1y}^2(\mathbf{r})] \bar{\alpha}_0^*(\mathbf{r}). \quad (25)$$

The knowledge of the variance (24) allows us to evaluate the possible effects of the DS movement on the noise detected, e.g., in a homodyning experiment. This could be quantitatively important as a possible noise reduction could be blurred by the diffusion of the structure [25].

D. Formal solution to the linearized Langevin equations

Now by substituting (20) into (6) and projecting onto $\{\mathbf{w}_i\}$, we obtain the evolution equation for the expansion coefficients in Eq. (20):

$$\dot{c}_i = \gamma_1 \lambda_i c_i + \sqrt{\gamma_1} \langle \mathbf{w}_i | \mathbf{h} \rangle, \quad (26)$$

where the index i does not include the Goldstone modes, as commented. We write down Eq. (26) in the temporal-frequencies space. By defining the Fourier transforms

$$c_i(t) = \frac{1}{2\pi} \int d\omega e^{i\omega t} \tilde{c}_i(\omega), \quad (27a)$$

$$\mathbf{h}(\mathbf{r}, t) = \frac{1}{2\pi} \int d\omega e^{i\omega t} \tilde{\mathbf{h}}(\mathbf{r}, \omega), \quad (27b)$$

and the corresponding inverse transforms

$$\tilde{c}_i(\omega) = \int dt e^{-i\omega t} c_i(t), \quad (28a)$$

$$\tilde{\mathbf{h}}(\mathbf{r}, \omega) = \int dt e^{-i\omega t} \mathbf{h}(\mathbf{r}, t), \quad (28b)$$

we find a simple expression in the temporal spectral domain for Eq.(26), that reads

$$i\omega \tilde{c}_i(\omega) = \gamma_1 \lambda_i \tilde{c}_i(\omega) + \sqrt{\gamma_1} \langle \mathbf{w}_i(\mathbf{r}) | \tilde{\mathbf{h}}(\mathbf{r}, \omega) \rangle, \quad (29)$$

which gives

$$\tilde{c}_i(\omega) = \frac{\sqrt{\gamma_1} \langle \mathbf{w}_i(\mathbf{r}) | \tilde{\mathbf{h}}(\mathbf{r}, \omega) \rangle}{i\omega - \gamma_1 \lambda_i}. \quad (30)$$

By using solution (30) in Eqs. (27), we retrieve the expansion coefficients $c_i(t)$

$$c_i(t) = \frac{\sqrt{\gamma_1}}{2\pi} \int d\omega e^{i\omega t} \frac{\langle \mathbf{w}_i(\mathbf{r}) | \tilde{\mathbf{h}}(\mathbf{r}, \omega) \rangle}{i\omega - \gamma_1 \lambda_i}, \quad (31)$$

which is the formal solution of the linearized Langevin equations, Eqs. (20) and (26) .

E. Modal correlation spectrum

Once the time-dependent expansion coefficients $c_i(t)$ are known, Eq. (31), we can calculate the two-time correlations between the different modes. The knowledge of these correlations, and specifically, of their spectra, is necessary in order to characterize some properties of quantum fluctuations, such as the spectrum of squeezing or the spectrum of intensity fluctuations of the quantum field exiting the nonlinear cavity, as will be shown below.

We define the correlation spectrum between two modes labeled by indices i and j as usual

$$S_{ij}(\omega) = \int d\tau e^{-i\omega\tau} \langle c_i(t + \tau), c_j(\tau) \rangle \quad (32)$$

where the correlation

$$\langle c_i(t + \tau), c_j(\tau) \rangle = \langle c_i(t + \tau) c_j(\tau) \rangle - \langle c_i(t) \rangle \langle c_j(t) \rangle, \quad (33)$$

and $\langle \mathcal{O} \rangle$ is the (stochastic) average value of \mathcal{O} . By using Eqs. (28) and (30), $S_{ij}(\omega)$ can be written as

$$S_{ij}(\omega) = \frac{\gamma_1}{2\pi} \int d\omega' \frac{e^{i(\omega' + \omega)\tau}}{(\gamma_1 \lambda_i - i\omega)(\gamma_1 \lambda_j - i\omega')} \times \langle \langle \mathbf{w}_i | \tilde{\mathbf{h}}(\mathbf{r}, \omega) \rangle, \langle \mathbf{w}_j | \tilde{\mathbf{h}}(\mathbf{r}, \omega) \rangle \rangle. \quad (34)$$

Taking into account the properties of noise, Eqs. (85), one obtains straightforwardly

$$\langle \langle \mathbf{w}_i | \tilde{\mathbf{h}}(\mathbf{r}, \omega) \rangle, \langle \mathbf{w}_j | \tilde{\mathbf{h}}(\mathbf{r}', \omega') \rangle \rangle = 2\pi \delta(\omega + \omega') \int d^2 r d_{ij}(\mathbf{r}, \mathbf{r}'), \quad (35)$$

where

$$d_{ij}(\mathbf{r}, \mathbf{r}) = w_i^*(\mathbf{r}) w_j^*(\mathbf{r}) \bar{\alpha}_0(\mathbf{r}) + [w_i^+(\mathbf{r})]^* [w_j^+(\mathbf{r})]^* \bar{\alpha}_0^*(\mathbf{r}), \quad (36)$$

so that the modal correlation spectrum $S_{ij}(\omega)$ can be written as

$$S_{ij}(\omega) = \frac{D_{ij}}{(\lambda_i - i\omega/\gamma_1)(\lambda_j + i\omega/\gamma_1)}, \quad (37)$$

where we have introduced the matrix D_{ij} , which we call modal diffusion matrix (because of the similarity of Eq. (37) with an spectral matrix [36]), defined by

$$D_{ij} = \int d^2 r d_{ij}(\mathbf{r}, \mathbf{r}). \quad (38)$$

Note that all modal correlations can be obtained just by diagonalizing the linear problem.

III. SQUEEZING SPECTRUM IN THE LINEAR APPROXIMATION

We consider now the squeezing properties of the classical DS $\bar{\mathcal{A}}_1$ as measured via a balanced homodyne detection experiment [21], which allows the direct measurement of quadrature squeezing. The quantum field outgoing the nonlinear cavity, to be denoted by $\hat{A}_{1,\text{out}}(\mathbf{r}, t)$, is combined at a beam splitter with a local oscillator field (LOF). This LOF lies in a classical multimode coherent state $\alpha_L(\mathbf{r} - \mathbf{r}_L(t))$ of intensity much larger than that of $\hat{A}_{1,\text{out}}(\mathbf{r}, t)$. (The shift $\mathbf{r}_L(t)$ is introduced in order to cover the case of a movable LOF for reasons that will be clear below, such as to consider the possibility to follow the DS movement.)

The difference $\hat{\Delta I}(t)$ between the intensities $\hat{\mathcal{D}}_+$ and $\hat{\mathcal{D}}_-$ of the two output ports of the beam splitter, with

$$\hat{\mathcal{D}}_{\pm}(\mathbf{r}, t) = \frac{1}{\sqrt{2}} [\hat{A}_{1,\text{out}}(\mathbf{r}, t) \pm \alpha_L(\mathbf{r} - \mathbf{r}_L(t))], \quad (39)$$

is then measured, and it turns out to be given by [21]

$$\begin{aligned} \hat{\Delta I}(t) &= \int d^2 r [\hat{\mathcal{D}}_+^\dagger(\mathbf{r}, t) \hat{\mathcal{D}}_+(\mathbf{r}, t) - \hat{\mathcal{D}}_-^\dagger(\mathbf{r}, t) \hat{\mathcal{D}}_-(\mathbf{r}, t)] \\ &\equiv \sqrt{N} \hat{E}_{\text{H,out}}(t). \end{aligned} \quad (40)$$

where the projection of the output signal field $\hat{A}_{1,\text{out}}(\mathbf{r}, t)$ on the LOF has been introduced as the field $\hat{E}_{\text{H,out}}(t)$

$$\hat{E}_{\text{H,out}}(t) = \hat{A}_{\text{H,out}}(t) + \hat{A}_{\text{H,out}}^\dagger(t), \quad (41)$$

$$\hat{A}_{\text{H,out}}(t) \equiv \frac{1}{\sqrt{N}} \int d^2 r \alpha_L^*(\mathbf{r} - \mathbf{r}_L(t)) \hat{A}_{1,\text{out}}(\mathbf{r}, t), \quad (42)$$

with the LOF intensity denoted by

$$N = \int d^2 r |\alpha_L(\mathbf{r})|^2. \quad (43)$$

By using (1), the spectrum of the difference intensity fluctuations can be written as

$$\begin{aligned} V(\omega) &= \int_{-\infty}^{\infty} d\tau e^{-i\omega\tau} \langle \hat{E}_{\text{H,out}}(t + \tau), \hat{E}_{\text{H,out}}(t) \rangle \\ &= 1 + \int_{-\infty}^{\infty} d\tau e^{-i\omega\tau} \langle : \hat{E}_{\text{H,out}}(t + \tau), \hat{E}_{\text{H,out}}(t) : \rangle \\ &= 1 + S_{\text{out}}(\omega), \end{aligned} \quad (44)$$

which defines the squeezing spectrum $S_{\text{out}}(\omega)$ of the field exiting the cavity. When $\hat{A}_{\text{out}}(\mathbf{r}, t)$ is in a coherent state, $V(\omega) = 1$ and $S_{\text{out}}(\omega) = 0$, which defines the standard quantum limit. Light is said to be squeezed at a frequency ω_c when $S_{\text{out}}(\omega_c) < 0$, and the case of complete noise reduction, or perfect squeezing, at ω_c is signaled by $S_{\text{out}}(\omega_c) = -1$ as in this case $V(\omega_c) = 0$.

Now the correlations of the output fields can be written in terms of those of the intracavity fields by using the input-output formalism [37]

$$\begin{aligned} \langle : \hat{A}_{1,\text{out}}^\dagger(t), \hat{A}_{1,\text{out}}(t') : \rangle &= 2\gamma_1 \langle : \hat{A}_1^\dagger(t), \hat{A}_1(t') : \rangle \\ &= 2\gamma_1 \langle \mathcal{A}_1^+(t), \mathcal{A}_1(t') \rangle \end{aligned} \quad (45)$$

and then

$$S_{\text{out}}(\omega) = 2\gamma_1 \int_{-\infty}^{\infty} d\tau e^{-i\omega\tau} \langle \delta \mathcal{E}_H(t + \tau), \delta \mathcal{E}_H(t) \rangle, \quad (46)$$

where $\delta \mathcal{E}_H(t) = \mathcal{E}_H(t) - \langle \mathcal{E}_H(t) \rangle$ with

$$\mathcal{E}_H(t) = \mathcal{A}_H(t) + \mathcal{A}_H^\dagger(t), \quad (47a)$$

$$\mathcal{A}_H(t) = \frac{1}{\sqrt{N}} \int d^2 r \alpha_L^*(\mathbf{r} - \mathbf{r}_L(t)) \mathcal{A}_1(\mathbf{r}, t). \quad (47b)$$

This expression can be written in a more compact form as

$$S_{\text{out}}(\omega) = \frac{2\gamma_1}{N} \int_{-\infty}^{\infty} d\tau e^{-i\omega\tau} \langle \delta\mathcal{E}_H(t+\tau) \delta\mathcal{E}_H(t) \rangle, \quad (48a)$$

$$\delta\mathcal{E}_H(t) = \langle \alpha_L(\mathbf{r} + \boldsymbol{\rho}(t)) | \mathbf{a}_1(\mathbf{r}, t) \rangle, \quad (48b)$$

where $\boldsymbol{\rho}(t) = \mathbf{r}_1(t) - \mathbf{r}_L(t)$, and the change of variables $\mathbf{r} \rightarrow \mathbf{r} - \mathbf{r}_1(t)$ has been introduced. (Remind that $\mathbf{r}_1(t)$ describes the position of the dissipative structure, that changes because of the diffusion introduced by quantum fluctuations, Eqs. (21).)

The output squeezing spectrum (48) can now be calculated in terms of the modal correlation spectrum (37): The intracavity field fluctuations $\mathbf{a}_1(\mathbf{r}, t)$ can be written in terms of the expansion (20) –remind that Goldstone modes are excluded–, so that the output squeezing spectrum (48) takes the form

$$S_{\text{out}}(\omega) = \frac{2\gamma_1}{N} \sum_{i,j} \langle \alpha_L | \mathbf{v}_i \rangle \langle \alpha_L | \mathbf{v}_j \rangle S_{ij}(\omega), \quad (49)$$

where

$$\begin{aligned} \langle \alpha_L | \mathbf{v}_i \rangle = & \int_{-\infty}^{\infty} d^2r \alpha_L^*(\mathbf{r} + \boldsymbol{\rho}(t)) v_i(\mathbf{r} + \mathbf{r}_1(t)) + \\ & \int_{-\infty}^{\infty} d^2r \alpha_L(\mathbf{r} + \boldsymbol{\rho}(t)) v_i^+(\mathbf{r} + \mathbf{r}_1(t)), \end{aligned} \quad (50)$$

and N and $S_{ij}(\omega)$ are given by Eqs. (43) and (37), respectively.

The projections of the eigenvectors \mathbf{v}_i onto the LOF are given by $\langle \alpha_L | \mathbf{v}_i \rangle$, where the scalar product (13) is used, and the modal correlation terms $S_{ij}(\omega)$ correspond to Eq.(37).

Up to this point we have treated with a complete detection of the beam, that is, we have considered an arbitrarily large detector covering the whole transverse profile of the outgoing field. We can wonder now on the effect of the detector size when it is finite, which corresponds to a more realistic description.

Thus we consider now a movable detector with finite transverse size Σ , which allows to sweep the transverse profile of the outgoing field and study the spatial distribution of squeezing. Mathematically, the use of a finite size detector corresponds to limit the spatial integrations in Eq. (49) to a domain Σ around the "detector position" \mathbf{r}_0 , so replacing $\langle \alpha_L | \mathbf{v}_i \rangle$, Eq. (50), by

$$\begin{aligned} \langle \alpha_L | \mathbf{v}_i \rangle_{\{\mathbf{r}_0, \Sigma\}} \equiv & \int_{\{\mathbf{r}_0, \Sigma\}} d^2r \alpha_L^*(\mathbf{r} + \boldsymbol{\rho}(t)) v_i(\mathbf{r} + \mathbf{r}_1(t)) + \\ & \int_{\{\mathbf{r}_0, \Sigma\}} d^2r \alpha_L(\mathbf{r} + \boldsymbol{\rho}(t)) v_i^+(\mathbf{r} + \mathbf{r}_1(t)), \end{aligned} \quad (51)$$

where $\{\mathbf{r}_0, \Sigma\}$ represents the spatial region occupied by the detector, and N , Eq. (43), by

$$N_{\{\mathbf{r}_0, \Sigma\}} \equiv \int_{\{\mathbf{r}_0, \Sigma\}} d^2r |\alpha_L(\mathbf{r})|^2. \quad (52)$$

Finally we can compute the squeezing spectrum measured when the finite detector is placed at \mathbf{r}_0 through

$$S_{\text{out}}(\omega; \mathbf{r}_0) = \frac{2\gamma_1}{N_{\{\mathbf{r}_0, \Sigma\}}} \times \sum_{i,j} \langle \alpha_L | \mathbf{v}_i \rangle_{\{\mathbf{r}_0, \Sigma\}} \langle \alpha_L | \mathbf{v}_j \rangle_{\{\mathbf{r}_0, \Sigma\}} S_{ij}(\omega). \quad (53)$$

As can be noted in Eq.(53), the obtained level of squeezing depends both on the area and position of the detector.

IV. INTENSITY FLUCTUATIONS SPECTRUM

Now we apply the technique used for calculating the squeezing spectrum to the derivation of spectrum of the intensity fluctuations. For the sake of simplicity here we ignore the diffusive movement of the DS, i.e., we assume that the detector can follow such motion.

The intensity fluctuations spectrum can be directly observed with a single photodetector and is given by [44]

$$V_I(\omega) = \int_{-\infty}^{\infty} dt e^{-i\omega t} \iint d^2r d^2r' \times \langle \delta \hat{I}_{\text{out}}(\mathbf{r}, t) \delta \hat{I}_{\text{out}}(\mathbf{r}', 0) \rangle, \quad (54)$$

where

$$\delta \hat{I}_{\text{out}}(\mathbf{r}, t) = \hat{I}_{\text{out}}(\mathbf{r}, t) - \langle \hat{I}_{\text{out}}(\mathbf{r}, t) \rangle, \quad (55)$$

and the term proportional to the intensity of the outgoing field is

$$\hat{I}_{\text{out}}(\mathbf{r}, t) = \hat{A}_{\text{out}}^\dagger(\mathbf{r}, t) \hat{A}_{\text{out}}(\mathbf{r}, t). \quad (56)$$

By making use of (1) and taking account of the input-output relation (45) one obtains [21]

$$V_I(\omega) = S_{\text{SN}} [1 + S_I(\omega)], \quad (57)$$

where the term corresponding to the shot noise reads

$$S_{\text{SN}} = 2\gamma_1 \int d^2r \langle \hat{I}_1(\mathbf{r}, t) \rangle, \quad (58)$$

and

$$S_I(\omega) = \frac{4\gamma_1^2}{S_{\text{SN}}} \int_{-\infty}^{\infty} dt e^{-i\omega t} \iint d^2r d^2r' \times \langle : \delta \hat{I}_1(\mathbf{r}, t) \delta \hat{I}_1(\mathbf{r}', 0) : \rangle, \quad (59)$$

where

$$\delta\hat{I}_1(\mathbf{r}, t) = \hat{I}_1(\mathbf{r}, t) - \langle \hat{I}_1(\mathbf{r}, t) \rangle, \quad (60a)$$

$$\hat{I}_1(\mathbf{r}, t) = \hat{A}_1^\dagger(\mathbf{r}, t)\hat{A}_1(\mathbf{r}, t). \quad (60b)$$

As stated, our interest is centered on the quantum fluctuations properties of the DS given by (5). When such form of the field is considered, the expression of the intensity fluctuations spectrum, leading to first order in fluctuations, reads

$$S_I(\omega) = \frac{2\gamma_1}{N} \int_{-\infty}^{\infty} d\tau e^{-i\omega\tau} \langle \delta\mathcal{E}_I(t+\tau) \delta\mathcal{E}_I(t) \rangle, \quad (61)$$

where

$$\delta\mathcal{E}_I(t) = \langle \bar{\mathbf{A}}_1(\mathbf{r}, t) | \mathbf{a}_1(\mathbf{r}, t) \rangle, \quad (62a)$$

$$\bar{N} = \int d^2r \langle |\bar{\mathbf{A}}_1(\mathbf{r})|^2 \rangle, \quad (62b)$$

$$\bar{\mathbf{A}}_1(\mathbf{r}) \equiv (\bar{\mathcal{A}}_1(\mathbf{r}), \bar{\mathcal{A}}_1^*(\mathbf{r}))^T. \quad (62c)$$

Notice that $\bar{\mathbf{A}}_1(\mathbf{r})$ is the vector which corresponds to the classical DS, given by Eq.(5).

As can be noted, the intensity fluctuations spectrum, Eq.(61), has the same expression as the squeezing spectrum, Eq.(48), but with the classical DS solution acting as LOF [21]. So, as it occurred previously with the output squeezing spectrum, the intensity fluctuations spectrum can be written in terms of the modal correlation spectrum (37)

$$S_I(\omega) = \frac{2\gamma_1}{N} \sum_{i,j} \langle \bar{\mathbf{A}}_1 | \mathbf{v}_i \rangle \langle \bar{\mathbf{A}}_1 | \mathbf{v}_j \rangle S_{ij}(\omega), \quad (63)$$

where

$$\langle \bar{\mathbf{A}}_1 | \mathbf{v}_i \rangle = \int_{-\infty}^{\infty} d^2r [\bar{\mathcal{A}}_1^*(\mathbf{r})v_i(\mathbf{r}) + \bar{\mathcal{A}}_1(\mathbf{r})v_i^+(\mathbf{r})]. \quad (64)$$

Finally, and analogously to what we did with the squeezing spectrum, when a finite detector of transverse size Σ positioned at \mathbf{r}_0 is considered the intensity fluctuations are given by Eq.(63) after replacing $\langle \bar{\mathbf{A}}_1 | \mathbf{v}_i \rangle$ by $\langle \bar{\mathbf{A}}_1 | \mathbf{v}_i \rangle_{\{\mathbf{r}_0, \Sigma\}}$ and \bar{N} by $\bar{N}_{\{\mathbf{r}_0, \Sigma\}}$ so that the intensity fluctuations spectrum measured with a finite detector of size Σ placed at \mathbf{r}_0 reads

$$S_I(\omega; \mathbf{r}_0) = \frac{2\gamma_1}{\bar{N}_{\{\mathbf{r}_0, \Sigma\}}} \times \sum_{i,j} \langle \bar{\mathbf{A}}_1 | \mathbf{v}_i \rangle_{\{\mathbf{r}_0, \Sigma\}} \langle \bar{\mathbf{A}}_1 | \mathbf{v}_j \rangle_{\{\mathbf{r}_0, \Sigma\}} S_{ij}(\omega), \quad (65)$$

where $\langle \bar{\mathbf{A}}_1 | \mathbf{v}_i \rangle_{\{\mathbf{r}_0, \Sigma\}}$ and $\bar{N}_{\{\mathbf{r}_0, \Sigma\}}$ are given, respectively, by Eqs.(51) and (52) when α_L is replaced by $\bar{\mathbf{A}}_1$.

V. A GENERAL RESULT ON THE SQUEEZING OF DISSIPATIVE STRUCTURES

Let us assume that we can set $\rho = 0$ in Eq. (50). This means that the LOF can be shifted in such a way that it exactly follows the diffusive movement of the dissipative structure whose squeezing is being to be measured. Further, let us choose the LOF $\alpha_L = \mathbf{w}_{2x}$, Eq. (19), i.e., a LOF whose shape is $\alpha_L = iG_x$. (We notice that the result that follows is valid for any α_L that corresponds to a linear combination of \mathbf{w}_{2x} and \mathbf{w}_{2y} .)

By doing this it turns out that $\delta\mathcal{E}_H(t) = c_{2x}(t)$, see Eqs. (20) and (48b). Standard techniques [28] applied to Eq. (26) for $i = 2x$

$$\dot{c}_{2x} = -2\gamma_1 c_{2x} + \sqrt{\gamma_1} \xi_{2x}, \quad (66)$$

where $\xi_{2x}(t) = \langle \mathbf{w}_{2x} | \mathbf{h} \rangle$ is the noise source and $c_{2x}(t) = \langle \mathbf{w}_{2x} | \mathbf{a}_1 \rangle$, allow the computation of the stochastic correlation $\langle \delta\mathcal{E}_H(t+\tau) \delta\mathcal{E}_H(t) \rangle$, that turns out to be

$$\langle \delta\mathcal{E}_H(t+\tau) \delta\mathcal{E}_H(t) \rangle = -\frac{1}{2} N_H e^{-2\gamma_1 |\tau|}. \quad (67)$$

Then, by using Eq. (48) we get

$$S_{\text{out}}(\omega) = -\frac{1}{1 + (\omega/2\gamma_1)^2}, \quad (68)$$

which is the main result in [25]. Of course the same result is obtained by using Eqs. (36), (37) and (38).

It is to be remarked that Eq. (66) is analogous to that derived in [45] for the stationary phase of the hexagonal mode appearing in the Kerr cavity model, and that it was later interpreted in [24] as the hexagonal pattern transverse linear momentum. Then we can say that the above result means that the transverse linear momentum of any stationary DS appearing in the large pump detuning limit of the DOPO model is perfectly squeezed in the linearized theory. This is a reasonable result as it is immediately related to the fact that the transverse position of the DS is completely undetermined as it diffuses with time.

Eq. (68) implies that $S(\omega = 0) = -1$ what means that within the validity domain of the linear theory we are using, any stationary dissipative structure sustained by the DOPO in the large pump detuning limit displays *perfect squeezing* at $\omega = 0$ when probed with the appropriate LOF. As Eq. (68) is independent of the kind of dissipative structure and of the system parameters, it is to be remarked that the result is universal and independent of the existence of bifurcations. Let us emphasize that the appropriate LOF ($\alpha_L = iG_{x(y)}$) is, in principle, easily implementable as it corresponds to the $\pi/2$ phase-shifted gradient of the corresponding DS envelope which can be easily synthesized by, e.g., Fourier filtering.

In [25] we discussed up to what extent the assumption $\rho = 0$ is reasonable: It is, indeed, as the diffusion of the dissipative structures is very slow because of the large number of photons they carry, which acts as an inertial mass [25].

We find it important to make here a general comment on the mathematical technique we have presented in the previous sections. We must note that the linearized approach we have presented is valid, in principle, when all eigenvalues are negative: In this case all fluctuations are damped and it is reasonable to assume that they will remain small enough. Remarkably, in our case there exists always two null eigenvalues, which are associated with the Goldstone modes (see Property 1 in Subsection II C). Nevertheless these null eigenvalues do not make the linear approach invalid as the undamped fluctuations do not concern any particular field mode but the position of the dissipative structure, which is decoupled from the rest of fluctuations and undergoes a continuous diffusion (as it occurs, e.g., with the phase difference in [7, 8]). Numerical research carried out in vectorial Kerr cavities [23] reinforce this confidence. In resume: In spite of having a null eigenvalue, we can be confident that the linearized description of quantum fluctuations will be reasonably accurate, and that a nonlinear treatment [22] will not lead to dramatically different results.

VI. SQUEEZING PROPERTIES OF THE DOPO BRIGHT CAVITY SOLITON

In this second part of the article, we study in detail the squeezing properties of the DOPO bright cavity soliton in the large pump detuning limit. First, in Subsection VI.A we review the main properties of this solution and then, in Subsection VI.B, we apply the theory developed in the first part to it. For the sake of simplicity we shall consider in this second part only the one-dimensional case, that is, we assume that the DOPO works embedded in a waveguide that avoids diffraction in the y transverse dimension whilst in the x transverse dimension the system aperture is arbitrarily large. Moreover, we shall assume from now on that the LOF used in the homodyne detection scheme can be moved, in the transverse dimension, in such a way that its movement exactly matches the diffusive motion of the bright cavity soliton, and thus we shall not take into account the diffusive motion of the DS (see [25] for a quantitative discussion in which we show that this is a reasonable assumption).

A. The DOPO bright cavity soliton

As stated in Subsection II.A, in the limit of large pump detuning we are considering here, the classical description of the DOPO is the PDNLSE, (Eq. (87) in Appendix B). It is well known that the one-dimensional PDNLSE supports two different types of localized structures (cavity solitons in our context): Dark cavity solitons (tanh-type localized structures) in the self-defocusing case $\sigma = -1$, and bright cavity solitons (sech-type localized structures) in the self-focusing case $\sigma = +1$ [39, 40, 41, 42]. We shall treat in the following the bright cavity soliton and thus

we take $\sigma = +1$.

Before going on we find it convenient to review the main solutions of the PDNLSE. This equation has only two free parameters (the parametric pump parameter μ and the cavity detuning Δ_1) as the rest of parameters (γ_1 , l_1 , and κ^2) can be easily removed by normalizing the time and space coordinates as well as the field amplitude (see Eq. (88) in Appendix B). When $\Delta_1 < 0$, the trivial state, $\bar{\mathcal{A}}_1(x) = 0$, undergoes a supercritical bifurcation towards a patterned state (a roll, or stripe, pattern) at $\mu = 1$. Contrarily, when $\Delta_1 > 0$ the bifurcation affecting the trivial state is subcritical and occurs at $\mu = \mu_0 \equiv \sqrt{1 + \Delta_1^2}$. For $\mu > \mu_0$, and positive Δ_1 , dynamic patterns are found [32].

The bright cavity soliton has the explicit expression

$$\bar{\mathcal{A}}_{1,BS}(x) = \sqrt{2}\beta e^{i\phi} \text{sech}(\beta x), \quad (69)$$

with

$$\beta^2 = \Delta_1 \pm \sqrt{\mu^2 - 1}, \quad (70a)$$

$$\cos(2\phi) = \mu^{-1}. \quad (70b)$$

This solution exists for $\Delta_1 > 0$ and $1 < \mu < \mu_0$ [43], and is stable in a wide domain of parameters, although for large enough Δ_1 it becomes unstable, through a Hopf bifurcation, thus appearing temporal oscillations (self-pulsing solitons) [33]. Then the bright cavity soliton can undergo three different bifurcations: (i) a tangent bifurcation at $\mu = 1$ (the BS does not exist for $\mu < 1$), (ii) a bifurcation at $\mu = \mu_0$ (the BS does not exist for $\mu > \mu_0$), and (iii) a Hopf bifurcation for large enough Δ_1 that transforms the stationary BS into a self-pulsing BS. In Fig. 1 we represent in the (Δ_1, μ) plane the domains of existence of the different solutions we have just commented.

It is convenient to briefly comment here on the similarities between the bright cavity soliton and the temporal soliton of the nonlinear Schrödinger equation (NLSE). The NLSE is a conservative equation that can be written without free parameters. Then, there is a family of sech-type solitons, that coexist, and for which certain quantities (such as the energy) are conserved. This is very different from the PDNLSE which is a nonconservative equation governed by two parameters. For given μ and Δ_1 , the sech-type solution is unique and can be stable or unstable. In fact the bright cavity soliton is not a true soliton and its name can be misleading when comparisons between these similar but actually quite different equations (NLSE and PDNLSE) are made. In particular, these differences manifest in the spectra of \mathcal{L} and \mathcal{L}^\dagger .

We have shown that in order to calculate the squeezing spectrum, given by Eq. (49), one needs to evaluate the spectra (12) of both \mathcal{L} and \mathcal{L}^\dagger (11) for $\bar{\mathcal{A}}_1(\mathbf{r}) = \bar{\mathcal{A}}_{1,BS}(x)$, Eq. (69). The spectrum of \mathcal{L} in this case has been extensively studied [42]. It consists of a continuous spectrum,

with eigenvalues of the form

$$\lambda_s(k) = -1 + s\sqrt{\mu^2 - \Delta_k^2}, \quad (71a)$$

$$\Delta_k = \Delta_1 + sk^2, \quad s = \pm 1, \quad k \in [0, \infty) \quad (71b)$$

and of a discrete spectrum with eigenvalues $\{\lambda_i\}_{i=1}^D$. The spectra of \mathcal{L} and \mathcal{L}^\dagger need to be computed numerically, as analytical expressions can not be derived in general, which we have done by adapting the Fourier method described in [43]. Nevertheless, some eigenvectors of the discrete spectrum can be computed analytically for some parameter sets. In particular, we have derived the four eigenvectors corresponding to the bifurcation occurring at $\mu = 1$. These eigenvectors are explicitly given in Appendix B.

A crucial point is whether the set of eigenvectors of \mathcal{L} and \mathcal{L}^\dagger form a (biorthonormal) basis or not. We commented above that for the similar problem of the nonlinear Schrödinger equation, describing temporal fiber solitons, the set of eigenvectors of \mathcal{L} and \mathcal{L}^\dagger do not form a base [11]. As in our case analytical expressions are not available, our strategy has consisted in discretizing the transverse spatial coordinate and numerically diagonalize \mathcal{L} and \mathcal{L}^\dagger . Our numerical results show that the number of independent eigenvectors coincides with the dimension of the matrices, what constitutes a numerical proof that for this particular transverse pattern, the eigenvectors of \mathcal{L} and \mathcal{L}^\dagger form a (biorthonormal) basis, whereas this does not happen in the conservative case. We see that the NLSE and the PDNLSE are very different problems indeed.

B. Squeezing properties of the unidimensional bright cavity soliton

Now we are in conditions for studying the squeezing properties of the DOPO bright cavity soliton. Of course the amount of squeezing to be obtained will depend on the local oscillator field (LOF) one uses in the homodyne measurements and, in general, on the parameter values (pump and detuning). We shall proceed in our study as follows: First, in Subsection VI.B.1, we shall particularize the general result obtained in [25] and derived above in Section III for the bright cavity soliton. Then, in Subsection VI.B.2, we shall consider the squeezing at the bifurcation points (which have been discussed in Subsection VI.A). Finally, in Subsection VI.B.3 we shall consider the case of a plane-wave LOF. In this last case we discuss first how the amount of squeezing changes with the parameters (for arbitrarily large detectors), and then how the level of squeezing depends on the size of the photodetectors when these have a finite transverse dimension.

1. Squeezing of the cavity soliton linear momentum

In Section VI we showed that there is a special mode that is perfectly squeezed in the linear approximation, which is equivalent to saying that the transverse linear momentum of the DS is perfectly squeezed. We saw that the fluctuations of this mode are detected by choosing the LOF $\alpha_L(x) = \mathbf{w}_{2x}(x)$, that is, $\alpha_L(\mathbf{r}) = i\partial_x \bar{\mathcal{A}}_{1,BS}(x)$, see Eq.(19). In Fig. 2 we represent the amplitude of this LOF with a dashed line together with the soliton amplitude, given by Eq. (69). (As the phase factor $\exp(i\phi)$ is space independent, Eq. (69), it has been discarded in making this plot.)

The similarity between $w_{2x}(x)$ and the Gauss–Hermite function

$$GH_1(x) \equiv ie^{i\phi} x e^{-\frac{1}{2}(x/\xi)^2}, \quad (72)$$

is immediate (in Fig. 2 the Gauss–Hermite function is also plotted), what suggests the use of this function, which is relatively easy to generate, as a LOF. In order to calculate the level of squeezing that would be detected by using the Gauss–Hermite LOF, Eq. (72), we take advantage of the general theory presented in the first part of this article: We expand the LOF on the basis of \mathcal{L}^\dagger as

$$\alpha_L = \sum_i \langle \mathbf{v}_i | \alpha_L \rangle \mathbf{w}_i, \quad (73)$$

excluding the Goldstone modes, and the squeezing spectrum is given by

$$S_{\text{out}}(\omega) = \frac{2\gamma}{N} \sum_{i,j} \langle \mathbf{v}_i | \alpha_L \rangle \langle \mathbf{v}_j | \alpha_L \rangle S_{ij}(\omega), \quad (74)$$

where the modal correlation matrix, Eq.(37), is evaluated from the computed spectra of \mathcal{L} and \mathcal{L}^\dagger . The accuracy of the numerical method was checked by computing $S_{\text{out}}(\omega)$ when $\alpha_L(x) = \mathbf{w}_2(x)$, yielding an error less than 10^{-13} . The influence of the Gauss–Hermite LOF width and position was already presented in [25], and we reproduce it in Fig. 3 for the sake of completeness. Notice that the level of squeezing is quite large even when the LOF position or width are not well matched to those of mode $\mathbf{w}_2(x)$.

2. Squeezing at the bifurcation points

At the bifurcations points there is, at least, one null eigenvalue, apart from that corresponding to the Goldstone mode. This implies the existence of a mode, different to $\mathbf{w}_2(x)$, whose eigenvalue reaches its minimum value. This mode is expected to be perfectly squeezed in the linear approximation. The squeezing of these modes is the equivalent to the usual squeezing at the bifurcation points that has been repeatedly studied in a large number of nonlinear cavities [3, 6].

We have seen that the bright cavity soliton can undergo three different bifurcations at $\mu = 1$, $\mu = \mu_0$, and $\mu = \mu_{\text{HB}}$, see Fig. 1. Let us consider first the bifurcation occurring at $\mu = 1$ (the analytic expression of the mode that has $\lambda = -2$ is given in the Appendix B, mode $\mathbf{w}_3(x)$). Then, by taking $\boldsymbol{\alpha}_L(x) = \mathbf{w}_3(x)$, one obtains the squeezing spectra that we have represented in Fig. 4 for $\Delta_1 = 1.2$ and three values of μ . Notice that $S_{\text{out}}(\omega = 0) = -1$ for $\mu = 1$ (full line); for $\mu = 1.0001$ (dashed line) the maximum squeezing does not reach -1 . Furthermore, as μ departs from unity the maximum squeezing does not occur at $\omega = 0$, but at a slightly different frequency. For $\mu = 1.01$, the maximum level of squeezing is close to -0.75 . That is, the squeezing degrades quickly as the system departs from this bifurcation. A similar behavior is exhibited at the bifurcation occurring at $\mu = \mu_0 = \sqrt{1 + \Delta_1^2}$ and we shall not enter into quantitative details.

Let us finally consider the Hopf bifurcation. For $\mu = \mu_{\text{HB}}$ there are two eigenmodes, let us denote them as $\mathbf{w}_{\text{HB}+}$ and $\mathbf{w}_{\text{HB}-}$, for which the eigenvalues read $\lambda_{\pm} = -2 \pm i\omega_{\text{HB}}$ (ω_{HB} is the oscillation frequency at the Hopf bifurcation), i.e., there are two most damped eigenmodes which are expected to exhibit maximum squeezing. But in the Hopf bifurcation there cannot be a LOF that matches these squeezed modes: Remind that the LOF vector was defined as $\boldsymbol{\alpha}_L = (\alpha_L, \alpha_L^*)^T$, and at the Hopf bifurcation the eigenvectors with $\text{Re } \lambda = -2$, $\mathbf{w}_{\text{HB}\pm} = (w_{\text{HB}\pm}, w_{\text{HB}\pm}^+)^T$, do not verify $w_{\text{HB}\pm}^+ = w_{\text{HB}\pm}^*$. This can be appreciated in Fig. 5 where we have represented the imaginary parts of $w_{\text{HB}+}^*$ and $w_{\text{HB}+}^+$ (also the real parts, not shown, are quite different). This fact makes it impossible to find a LOF such that $(\boldsymbol{\alpha}_L | \mathbf{v}_{\text{HB}}) = 1$. Then perfect noise reduction is never achieved at the Hopf bifurcation.

The amount of squeezing attainable at the Hopf bifurcation is represented in Fig. 6 where the squeezing spectrum has been represented for two choices of the LOF: $\boldsymbol{\alpha}_L(x) = \mathbf{w}_{\text{HB}+}(x)$, in dashed line, and $\boldsymbol{\alpha}_L(x) = \mathbf{w}_{\text{HB}+}(x) + \mathbf{w}_{\text{HB}-}(x)$, in full line. Interestingly the maximum squeezing is larger for the latter choice. Notice also that, in contrast to the other bifurcations and as it is well known, at the Hopf bifurcation the maximum level of squeezing is reached at a frequency different from $\omega = 0$, which corresponds to the self-pulsing frequency of the bright cavity soliton.

3. Squeezing with a plane-wave local oscillator

We consider now the particular case of the squeezing properties of the bright cavity soliton when measured in a homodyning experiment, probed with a plane-wave LOF, which is of obvious relevant interest as this is the simplest LOF.

At a first stage we deal, as in the preceding subsections, with a complete beam detection, that is, the detector is assumed to completely cover the transverse ex-

tension of the outgoing quantum cavity soliton. Fig. 7 shows the squeezing spectra obtained for five different values of the pump μ and $\Delta_1 = 1.2$. The maximum of squeezing is achieved at frequency $\omega = 0$ irrespective of the pump value (which is obviously limited to $1 < \mu < \mu_0 = \sqrt{1 + \Delta_1^2}$, see Fig. 1). A high degree of squeezing, sustained for a large range of parameters setting, is obtained. This is more clearly seen in the inset of Fig. 7, where $S(\omega = 0)$ is depicted as a function of pump for $\Delta_1 = 1.2$.

We have also calculated the influence of the detuning: In Fig. 8 we plot the same as in Fig. 7 but for fixed $\mu = 1.2$ and as a function of detuning Δ_1 . Again large squeezing levels are obtained in all the domain of existence of the cavity soliton (for detunings larger than those represented in Fig. 8, the cavity soliton becomes Hopf unstable as already commented).

We focus now on the homodyning detection when using finite size detectors. When a detector, with size Σ and positioned at $x = x_0$ is used, the squeezing spectrum detected is given by Eq. (53), particularized to the BS solution. In the particular case of a plane-wave LOF, the calculations are considerably simplified, as $\boldsymbol{\alpha}_L$ is constant. We note, as well, that the phase of the plane-wave LOF is a free parameter, which is allowed to vary in order to obtain the maximum level of squeezing.

In Fig. 9, we represent the spatial distribution of squeezing, for $\mu = \Delta_1 = 1.2$ and at $\omega = 0$, when the finite size detector is displaced across the transverse dimension. We consider three different values of the detector size $\Sigma = \Delta x / \beta$ normalized to the BS width β , see Eq. (70a), as indicated in the figure. In the three cases the phase of the plane-wave LOF (not shown) has been chosen in order to obtain the maximum squeezing at each position of the detector in the transverse plane. A clear conclusion can be extracted from these plots: The smaller is the detector size, the smaller is the squeezing level one attains. This is to be expected as the smaller the photodetector is, the larger influence of high spatial frequency modes, i.e., with the smaller photodetector the influence of all sort of nonsqueezed modes is larger than with the larger photodetectors which filter out high frequency modes. One more conclusion one can extract from the figure is that the squeezing level is larger, for all detector sizes, at the center of the soliton ($x = 0$), i.e., the soliton is more squeezed than the vacuum (for large x the soliton amplitude tends to zero and the squeezing is due to the squeezed vacuum).

Finally we focus on the influence of the detector size on the degree of squeezing reached when the detector is placed at the exact center of the soliton. Fig. 10 shows the maximum squeezing reached in these conditions at frequency $\omega = 0$ when a detector of normalized size Σ is considered. Several features can be appreciated in the figure. As a general trend, the squeezing level degrades as the detector size is reduced, i.e., the maximum level of squeezing is found for a very large detector. But, interestingly, for $1.5 < \Sigma < 3$, the squeezing decreases with

the increase of the detector size. Obviously, for detectors whose size falls in this region what is happening is that the fluctuations being detected come from both the BS and the trivial solution (below threshold emission) existing far from the detector. In fact we see that the phase of the local oscillator that optimizes the squeezing level (represented with a dashed line, left vertical axis), which is almost insensitive to the detector size for $\Sigma < 1$, changes rapidly in this detector width region. Then, for large detectors, $\Sigma > 10$, the monotonic increase of squeezing with the detector width is recovered and the optimum phase for the LOF is again almost insensitive to the detector size.

VII. CONCLUSIONS

In this article we have developed a general theory for the analysis of linearized quantum fluctuations of optical dissipative structures generated in wide aperture nonlinear optical cavities. Although we have done this explicitly for the special case of the degenerate optical parametric oscillator in the large pump detuning limit, our method can be easily generalized to any other nonlinear cavity. The method consists, in short, in expanding the fluctuations in the biorthonormal base that the eigenvectors of the linear deterministic operator of the linearized Langevin equations of the system. This technique allows, in particular, the identification of a special mode which is perfectly squeezed (in the linear approximation). The perfect squeezing occurs irrespective of the nonlinear cavity parameter values, and the special mode can be identified with the transverse linear momentum of the dissipative structure that is being emitted. It must be emphasized that the existence of this squeezed mode is a genuine transverse effect, i.e., it is associated to the symmetry breaking introduced by the existence of dissipative structures.

Then we have applied this theory to the study of squeezing of a particular dissipative structure, namely, the bright cavity soliton. In particular we have analyzed the squeezing occurring at the different bifurcations that this dissipative structure can undergo at the same time that the appropriate LOF for detecting it in each situation. Then we have studied the squeezing detected when a plane wave LOF is used and analyzed its dependence on the parameter values. Finally we have considered also finite size detectors. We have shown that for large detectors the squeezing level is large almost independently of the system parameters. For finite size detectors, we have analyzed the spatial distribution of squeezing.

We gratefully acknowledge fruitful discussions with A. Gatti, K. Staliunas and J. A. de Azcárraga. This work has been supported by the Spanish Ministerio de Educación y Ciencia and the European Union FEDER through Projects BFM2002-04369-C04-01, FIS2005-07931-C03-01 and -02 and Programa Juan de la Cierva.

VIII. APPENDIX A

In this Appendix the DOPO model used along the paper is derived. The Hamiltonian describing the DOPO in the interaction picture is given by [26]

$$\hat{H} = \hat{H}_{\text{free}} + \hat{H}_{\text{int}} + \hat{H}_{\text{ext}}, \quad (75)$$

where

$$\hat{H}_{\text{free}} = \hbar \sum_{n=0,1} \gamma_n \int d^2r \hat{A}_n^\dagger (\Delta_n - l_n^2 \nabla^2) \hat{A}_n, \quad (76)$$

governs the free evolution of the intracavity fields in the paraxial approximation,

$$\hat{H}_{\text{int}} = \frac{\hbar g}{2} \int d^2r i \left[\hat{A}_0 (\hat{A}_1^\dagger)^2 - \hat{A}_0^\dagger (\hat{A}_1)^2 \right], \quad (77)$$

describes the nonlinear interaction, and

$$\hat{H}_{\text{ext}} = \hbar \int d^2r i \left[\mathcal{E}_{\text{int}} \hat{A}_0^\dagger - \mathcal{E}_{\text{int}}^* \hat{A}_0 \right], \quad (78)$$

accounts for the coherent driving. In the above expressions $l_n = c/\sqrt{2\omega_n\gamma_n}$ is the diffraction length for the field \hat{A}_n , $\Delta_0 = (\omega_0 - 2\omega_s)/\gamma_0$ and $\Delta_1 = (\omega_1 - \omega_s)/\gamma_1$ are the (adimensional) pump and signal detuning parameters, respectively, $\nabla^2 = \partial^2/\partial x^2 + \partial^2/\partial y^2$ is the transverse Laplacian operator, and g is the (real) nonlinear coupling coefficient, given by

$$g = \frac{3\chi^{(2)}\omega_s}{2(2\pi n)^3} \sqrt{\frac{\hbar\omega_s}{\varepsilon_0 L_z}}, \quad (79)$$

with $\chi^{(2)}$ the relevant nonlinear susceptibility matrix element, n the common value of the refractive index of the crystal at pump and signal wavelengths (a type I DOPO is considered), and L_z the thickness of the crystal along the resonator axis.

From the above Hamiltonian one obtains the master equation governing the evolution of the density matrix $\hat{\rho}$ of the intracavity modes,

$$\frac{\partial}{\partial t} \hat{\rho} = \frac{1}{i\hbar} [\hat{H}, \hat{\rho}] + \hat{\Lambda} \hat{\rho}, \quad (80)$$

where the Liouvillian term

$$\hat{\Lambda} \hat{\rho} = \sum_{n=0,1} \gamma_n \int d^2r \left[2\hat{A}_n(\mathbf{r}, t) \hat{\rho} \hat{A}_n^\dagger(\mathbf{r}, t) - \hat{\rho} \hat{A}_n^\dagger(\mathbf{r}, t) \hat{A}_n(\mathbf{r}, t) - \hat{A}_n(\mathbf{r}, t) \hat{A}_n^\dagger(\mathbf{r}, t) \hat{\rho} \right], \quad (81)$$

models the coupling between the system and the external reservoir through the output mirror.

Passing to the the generalized P representation [27] one can transform the master equation (80) into an equivalent Fokker-Planck equation for a quasiprobability density (denoted by P), following standard methods (see, e.g. [26]), the result being:

$$\begin{aligned}
\frac{\partial}{\partial t} P(\mathbf{A}) = & \left\{ \int d^2r \left[\frac{\partial}{\partial \mathcal{A}_0} \left(-\gamma_0 L_0 \mathcal{A}_0 + \frac{g}{2} \mathcal{A}_1^2 - \mathcal{E}_{\text{in}} \right) + \right. \right. \\
& \frac{\partial}{\partial \mathcal{A}_0^+} \left(-\gamma_0 L_0^* \mathcal{A}_0^+ + \frac{g}{2} \mathcal{A}_1^{+2} - \mathcal{E}_{\text{in}}^* \right) + \\
& \frac{\partial}{\partial \mathcal{A}_1} \left(-\gamma_1 L_1 \mathcal{A}_1 - g \mathcal{A}_1^+ \mathcal{A}_0 \right) + \\
& \frac{\partial}{\partial \mathcal{A}_1^+} \left(-\gamma_1 L_1^* \mathcal{A}_1^+ - g \mathcal{A}_1 \mathcal{A}_0^+ \right) + \\
& \left. \frac{g}{2} \left(\frac{\partial^2}{\partial \mathcal{A}_1^2} \mathcal{A}_0 + \frac{\partial^2}{\partial \mathcal{A}_1^{+2}} \mathcal{A}_0^+ \right) \right] \Big\} P(\mathbf{A}). \quad (82)
\end{aligned}$$

In the above expression $\mathbf{A} = (\mathcal{A}_0, \mathcal{A}_0^+, \mathcal{A}_1, \mathcal{A}_1^+)$, and

$$L_j = -(1 + i\Delta_j) + il_j^2 \nabla^2. \quad (83)$$

In its turn, a Fokker-Planck equation, here Eq. (82), can be transformed into an equivalent classical-looking set of stochastic differential equations (so called Langevin equations) via Ito rules [28]. In our case they read

$$\frac{\partial}{\partial t} \mathcal{A}_0 = \gamma_0 L_0 \mathcal{A}_0 - \frac{g}{2} \mathcal{A}_1^2 + \mathcal{E}_{\text{in}}, \quad (84a)$$

$$\frac{\partial}{\partial t} \mathcal{A}_0^+ = \gamma_0 L_0^* \mathcal{A}_0^+ - \frac{g}{2} \mathcal{A}_1^{+2} + \mathcal{E}_{\text{in}}^*, \quad (84b)$$

$$\frac{\partial}{\partial t} \mathcal{A}_1 = \gamma_1 L_1 \mathcal{A}_1 + g \mathcal{A}_1^+ \mathcal{A}_0 + \sqrt{g \mathcal{A}_0} \eta(\mathbf{r}, t), \quad (84c)$$

$$\frac{\partial}{\partial t} \mathcal{A}_1^+ = \gamma_1 L_1^* \mathcal{A}_1^+ + g \mathcal{A}_1 \mathcal{A}_0^+ + \sqrt{g \mathcal{A}_0^+} \eta^+(\mathbf{r}, t), \quad (84d)$$

with $\eta(\mathbf{r}, t)$ and $\eta^+(\mathbf{r}, t)$ independent, real white Gaussian noises of zero average and correlations given by

$$\langle \eta^+(\mathbf{r}', t'), \eta(\mathbf{r}, t) \rangle = 0, \quad (85a)$$

$$\langle \eta^+(\mathbf{r}, t), \eta^+(\mathbf{r}', t') \rangle = \delta(\mathbf{r} - \mathbf{r}') \delta(t - t'), \quad (85b)$$

$$\langle \eta(\mathbf{r}, t), \eta(\mathbf{r}', t') \rangle = \delta(\mathbf{r} - \mathbf{r}') \delta(t - t'). \quad (85c)$$

Note that, if \mathcal{A}_i^+ is interpreted as \mathcal{A}_i^* and the noise terms are ignored (classical limit), Eqs. (84) coincide with the classical equations for a planar DOPO [29].

Equations (84) are already set in a convenient way to apply the method we develop in this paper. However we shall use a simpler form of them obtained in the limit of large pump detuning, defined by $|\Delta_0| \gg 1, \gamma_0/\gamma_1, |\Delta_1|$, which allows the adiabatic elimination of the pump field [30, 31] as

$$\mathcal{A}_0 = \mathcal{A}_{0,\text{ad}} \equiv \frac{-i}{\gamma_0 \Delta_0} \left(\mathcal{E}_{\text{in}} - \frac{g}{2} \mathcal{A}_1^2 \right), \quad (86a)$$

$$\mathcal{A}_0^+ = \mathcal{A}_{0,\text{ad}}^+ \equiv \frac{i}{\gamma_0 \Delta_0} \left(\mathcal{E}_{\text{in}}^* - \frac{g}{2} \mathcal{A}_1^{+2} \right). \quad (86b)$$

We note that these expressions correct some typos appearing in the corresponding expressions in [25]. The remaining Langevin equations for the signal field are obtained by substitution of the limit solution (86) into (84).

By taking, without loss of generality, the external pump field amplitude as a purely imaginary quantity whose imaginary part has the same sign as the pump detuning Δ_0 , i.e. $\mathcal{E}_{\text{in}} = i\sigma |\mathcal{E}_{\text{in}}|$ with $\sigma = \text{sign } \Delta_0$, they become Eqs. (2) in Sec. II A, which is the model we shall consider.

IX. APPENDIX B

In the classical limit ($\mathcal{A}_1^+ \rightarrow \mathcal{A}_1^*$, and $\eta, \eta^+ \rightarrow 0$), Eqs. (2) reduce to

$$\frac{\partial}{\partial t} \mathcal{A}_1(\mathbf{r}, t) = \gamma_1 \left(L_1 \mathcal{A}_1 + \mu \mathcal{A}_1^* + i \frac{\sigma}{\kappa^2} |\mathcal{A}_1|^2 \mathcal{A}_1 \right), \quad (87)$$

$L_1 = -(1 + i\Delta_1) + il_1^2 \nabla^2$, which is a version of the so called parametrically driven, nonlinear Schrödinger equation (PDNLSE), which is a universal model for pattern formation in parametrically driven systems (see, e.g., [35] for a list of systems described by the PDNLSE). A convenient normalization of that equation is obtained by introducing the following dimensionless quantities: time $T = \gamma_1 t$, spatial coordinates $(X, Y) = (x/l_1, y/l_1)$, and field $\psi = \mathcal{A}_1/\kappa$, so that Eq. (87) becomes

$$\partial_T \psi = \mu \psi^* - (1 + i\Delta_1) \psi + i(\partial_X^2 + \partial_Y^2) \psi + i\sigma |\psi|^2 \psi. \quad (88)$$

For the bright cavity soliton, Eq. (69), operators \mathcal{L} and \mathcal{L}^\dagger take the form

$$\mathcal{L} = \begin{pmatrix} \mathcal{L}_1 & \bar{\mathcal{A}}_0 \\ \bar{\mathcal{A}}_0^* & \mathcal{L}_1^* \end{pmatrix}, \quad \mathcal{L}^\dagger = \begin{pmatrix} \mathcal{L}_1^* & \bar{\mathcal{A}}_0 \\ \bar{\mathcal{A}}_0^* & \mathcal{L}_1 \end{pmatrix}, \quad (89a)$$

where

$$\mathcal{L}_1 = -(1 + i\Delta_1) + i\nabla^2 + i \left(\frac{2\beta}{\kappa} \right)^2 \text{sech}^2(\beta x), \quad (90a)$$

$$\bar{\mathcal{A}}_0 = \mu + i \left(\frac{2\beta}{\kappa} \right)^2 e^{2i\phi} \text{sech}^2(\beta x) \quad (90b)$$

and

$$\beta^2 = \Delta_1 \pm \sqrt{\mu^2 - 1}, \quad (91a)$$

$$\cos(2\phi) = \mu^{-1}. \quad (91b)$$

Then, for $\mu = 1$ one can calculate the discrete eigenvalues analytically. The result is that the discrete eigenvectors of \mathcal{L} and \mathcal{L}^\dagger with null eigenvalue are

$$\mathbf{v}_1 = -S \mathcal{T} \begin{pmatrix} e^{i\phi} \\ e^{-i\phi} \end{pmatrix}, \quad (92a)$$

$$\mathbf{w}_1 = -S \begin{pmatrix} (x + i\mathcal{T}) e^{i\phi} \\ (x - i\mathcal{T}) e^{-i\phi} \end{pmatrix}, \quad (92b)$$

$$\mathbf{v}_4 = i\beta^{-1/2} S \begin{pmatrix} [\beta^2 + i(x\mathcal{T} - 1)] e^{i\phi} \\ -[\beta^2 - i(x\mathcal{T} - 1)] e^{-i\phi} \end{pmatrix}, \quad (92c)$$

$$\mathbf{w}_4 = \beta^{1/2} S \begin{pmatrix} e^{i\phi} \\ e^{-i\phi} \end{pmatrix}, \quad (92d)$$

and that the discrete eigenvectors of \mathcal{L} and \mathcal{L}^\dagger with eigenvalue $\lambda = -2$ are

$$\mathbf{v}_2 = -i\beta^{1/2} \mathcal{S} \begin{pmatrix} (x + i\mathcal{T}) e^{i\phi} \\ -(x - i\mathcal{T}) e^{-i\phi} \end{pmatrix}, \quad (93a)$$

$$\mathbf{w}_2 = -i\beta^{-1/2} \mathcal{S} \mathcal{T} \begin{pmatrix} e^{i\phi} \\ -e^{-i\phi} \end{pmatrix}, \quad (93b)$$

$$\mathbf{v}_3 = i\beta \mathcal{S} \begin{pmatrix} e^{i\phi} \\ -e^{-i\phi} \end{pmatrix}, \quad (93c)$$

$$\mathbf{w}_3 = -\beta^{-1} \mathcal{S} \begin{pmatrix} [\beta^2 + i(x\mathcal{T} - 1)] e^{i\phi} \\ [\beta^2 - i(x\mathcal{T} - 1)] e^{-i\phi} \end{pmatrix}. \quad (93d)$$

In the above expressions \mathbf{v}_1 is the Goldstone mode, Eq. (7), and we have introduced the quantities

$$\mathcal{S} = \sqrt{\frac{\beta}{2}} \operatorname{sech}(\beta x), \quad \mathcal{T} = \beta \tanh(\beta x). \quad (94)$$

Let us finally notice that for $\mu = 1$, it turns out that $\beta^2 = \Delta_1$ and $\cos(2\phi) = 1$.

-
- [1] P. D. Drummond and Z. Ficek (eds.), *Quantum Squeezing* (Springer, 2004).
- [2] R. Loudon and P. L. Knight, J. Mod. Opt. **34**, 709 (1987).
- [3] P. Meystre and D. F. Walls (eds.), *Nonclassical Effects in Quantum Optics* (American Institute of Physics, New York, 1991).
- [4] N. Korolkova, G. Leuchs, R. Loudon, T. C. Ralph, and Ch. Silberhorn, Phys. Rev. A **65**, 052306 (2002).
- [5] V. V. Dodonov and V. I. Man'ko (eds.), *Theory of Nonclassical States of Light*, (Taylor and Francis, London, 2003).
- [6] D. F. Walls and G. J. Milburn, *Quantum Optics*, (Springer Verlag, Berlin, 1994).
- [7] S. Reynaud, C. Fabre, and E. Giacobino, J. Opt. Soc. Am. B **4**, 1520 (1987).
- [8] M. D. Reid and P. D. Drummond, Phys. Rev. Lett. **60**, 2371 (1988).
- [9] P. D. Drummond and S. J. Carter, J. Opt. Soc. Am. **4**, 1565 (1987).
- [10] H. A. Haus and Y. Lai, J. Opt. Soc. Am. B **7**, 386 (1990).
- [11] V. V. Kozlov, IEEE J. Sel. Topics Quant. Electron. **9**, 1468 (2003).
- [12] N. Treps and C. Fabre, Phys. Rev. A **62**, 033816 (2000).
- [13] E. Lantz, T. Sylvestre, H. Maillotte, N. Treps, and C. Fabre, J. Opt. B: Quantum Semiclass. Opt. **6**, S295 (2004).
- [14] E. M. Nagasako, R. W. Boyd, and G. S. Agarwal, Opt. Express **3**, 171 (1998).
- [15] A. Mecozzi and P. Kumar, Quantum Semiclass. Opt. **10**, 21 (1998).
- [16] L. A. Lugiato, M. Brambilla, and A. Gatti, *Optical Pattern Formation*, Adv. Atom. Mol. Opt. Phys. **40**, 229 (1999).
- [17] L. A. Lugiato, A. Gatti, and E. Brambilla, J. Opt. B: Quantum Semiclass. Opt. **4**, S176 (2002).
- [18] M. I. Kolobov, Rev. Mod. Phys. **71**, 1539 (1999).
- [19] L. A. Lugiato and G. Grynberg, Europhys. Lett. **29**, 675 (1995).
- [20] L. A. Lugiato and A. Gatti, Phys. Rev. Lett. **70**, 3868 (1993).
- [21] A. Gatti and L. A. Lugiato, Phys. Rev. A **52**, 1675 (1995).
- [22] P. D. Drummond and K. Dechoum, Phys. Rev. Lett. **95**, 083601 (2005).
- [23] R. Zambrini, M. Hoyuelos, A. Gatti, P. Colet, L. A. Lugiato, and M. San Miguel, Phys. Rev. A **62**, 063801 (2002).
- [24] D. Gomila and P. Colet, Phys. Rev. E **66**, 046223 (2002).
- [25] I. Pérez-Arjona, E. Roldán, and G. J. de Valcárcel, Europhys. Lett. **74**, 247 (2006).
- [26] A. Gatti, H. Wiedemann, L. A. Lugiato, I. Marzoli, G. L. Oppo, and S. M. Barnett, Phys. Rev. A **56**, 877 (1997).
- [27] P. D. Drummond and C. W. Gardiner, J. Phys. A **13**, 2353 (1980).
- [28] C. W. Gardiner and P. Zoller, *Quantum Noise* (Springer, 2000).
- [29] G. L. Oppo, M. Brambilla, and L. A. Lugiato, Phys. Rev. A **49**, 2028 (1994).
- [30] S. Longhi, Phys. Scr. **56**, 611 (1997).
- [31] S. Trillo, M. Haelterman, and C. Sheppard, Opt. Lett. **22**, 970 (1997).
- [32] S. Longhi and A. Geraci, Appl. Phys. Lett. **67**, 3060 (1995).
- [33] M. Bondila, I. V. Barashenkov, and M. M. Bogdan, Physica D **87**, 314 (1995).
- [34] I. V. Barashenkov, N. V. Alexeeva, and E. V. Zemlyanaya, Phys. Rev. Lett. **89**, 104101 (2002).
- [35] G. J. de Valcárcel, I. Pérez-Arjona, and E. Roldán, Phys. Rev. Lett. **89**, 164101 (2002).
- [36] M. J. Collet and D. F. Walls, Phys. Rev. A **32**, 2887 (1985).
- [37] M. J. Collet and C. W. Gardiner, Phys. Rev. A **30**, 1386 (1984).
- [38] N. Alexeeva, I. V. Barashenkov, and G. P. Tsironis, Phys. Rev. Lett. **84**, 3053 (2000).
- [39] S. Fauve and O. Thual, Phys. Rev. Lett. **64**, 282 (1990).
- [40] J. W. Miles, J. Fluid Mech. **148**, 451 (1984).
- [41] C. Elphick and E. Meron, Phys. Rev. A **40**, 3226 (1989).
- [42] I. V. Barashenkov, M. M. Bogdan, and V. I. Korobov, Europhys. Lett. **15**, 113 (1991).
- [43] N. V. Alexeeva, I. V. Barashenkov and D. E. Pelinovsky, Nonlinearity **12**, 103 (1999).
- [44] R. J. Glauber, Phys. Rev. **130**, 2529 (1963); *ibid.* **131**, 2766 (1963).
- [45] A. Gatti and S. Mancini, Phys. Rev. A **65**, 013816 (2001).

FIGURE CAPTIONS

Fig.1. Schematic representation of the different patterns one finds in the PDNLSE, Eq. (88). The line μ_{HB} has been plotted after the numerical results of [33].

Fig.2. Amplitude of the bright cavity soliton, Gauss-Hermite mode (GH_1), and the mode w_2 (in dashed line).

Fig.3. Squeezing level (at the labeled frequencies) displayed by the bright cavity soliton when a Gauss-Hermite mode (GH_1) or mode w_2 (see text) is used as a LOF. In (a) a GH_1 of width ξ is used. In (b) the LOF is displaced x from the CS center. Parameters are $\Delta_1 = 1$, and $\mu = 1.2$.

Fig.4. Squeezing spectra close to the tangent bifurcation at $\mu = 1.0$. The detuning parameter is $\Delta_1 = 1.2$ and the pump values are indicated in the figure.

Fig.5. Imaginary parts of w_{HB+}^* (full line) and w_{HB+}^+ (dashed line). See text.

Fig.6. Squeezing spectrum at Hopf bifurcation. The dashed line corresponds to using one of the two most damped modes (with $\text{Re } \lambda = 0$) at this bifurcation as LOF. The full line corresponds to using as LOF the sum

of these two modes.

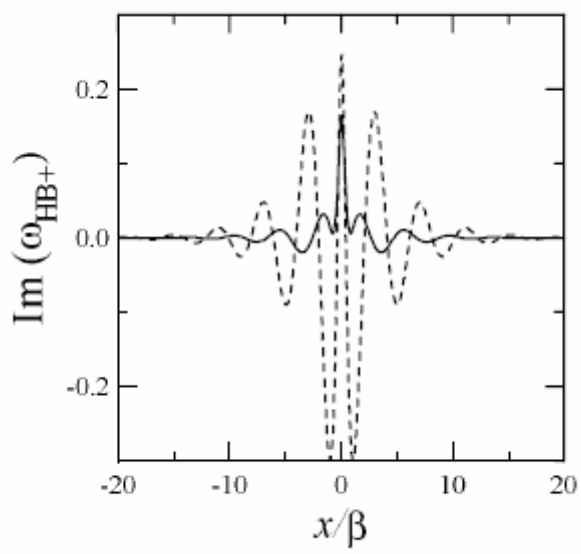
Fig.7. Squeezing spectra obtained when using a plane-wave LOF. The detuning parameter is $\Delta_1 = 1.2$ and the pump value is indicated in the figure. In the inset the maximum squeezing at $\omega = 0$ is represented as a function of pump for the same detuning value.

Fig.8. Squeezing spectra obtained when using a plane-wave LOF. The pump parameter is $\mu = 1.2$ and the detuning value is indicated in the figure. In the inset the maximum squeezing at $\omega = 0$ is represented as a function of detuning for the same pump parameter value.

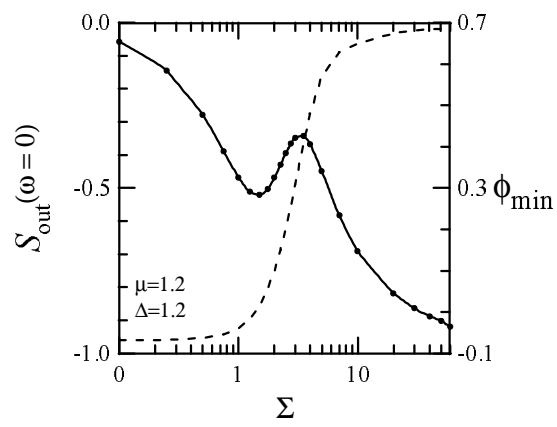
Fig.9. Spatial distribution of the squeezing when probed with a plane-wave LOF and measured with finite size detectors of normalized size $\Sigma = \Delta x / \beta$ (the values are marked in the figure). The phase of the LOF has been chosen in order to obtain the maximum noise reduction at each detector position. Parameters are $\mu = \Delta_1 = 1.2$.

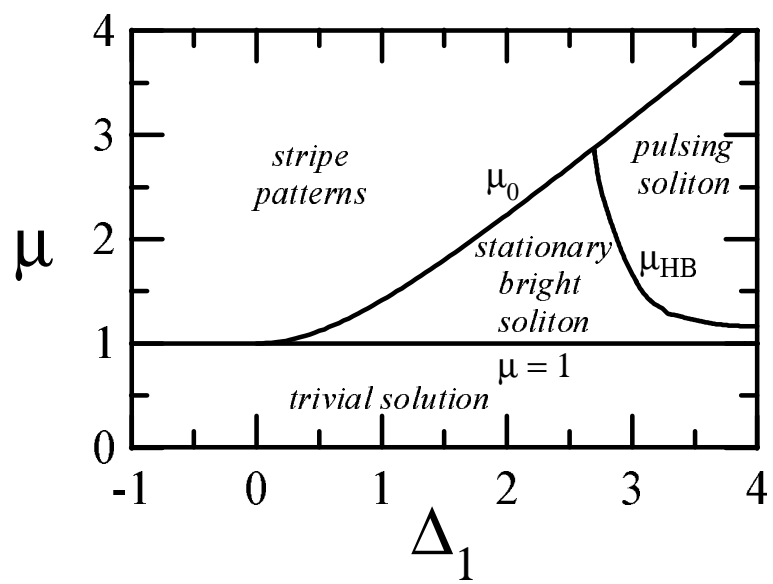
Fig.10. Maximum squeezing S_{out} at $\omega = 0$, obtained with a finite size detector centered at the BS center, as a function of the detector size $\Sigma = \Delta x / \beta$. Parameters are $\mu = \Delta_1 = 1.2$.

Pérez-Arjona et al.
"Theory of quantum fluctuations..."
Fig.5

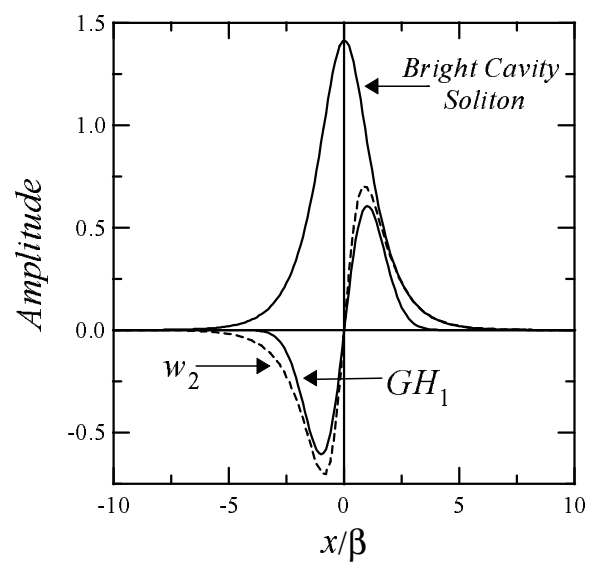


Pérez-Ajona et al.
 "Theory of quantum fluctuations..."
 Fig. 10



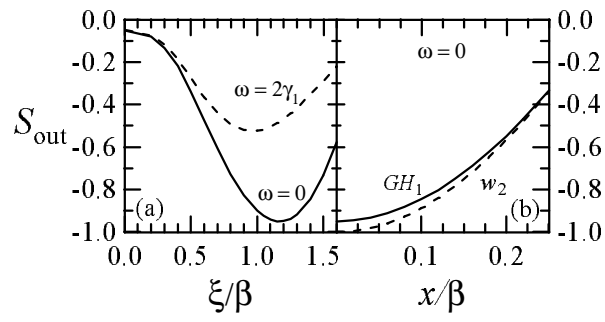


Pérez-Arjona et al.
 "Theory of quantum fluctuations..."
 Fig. 1

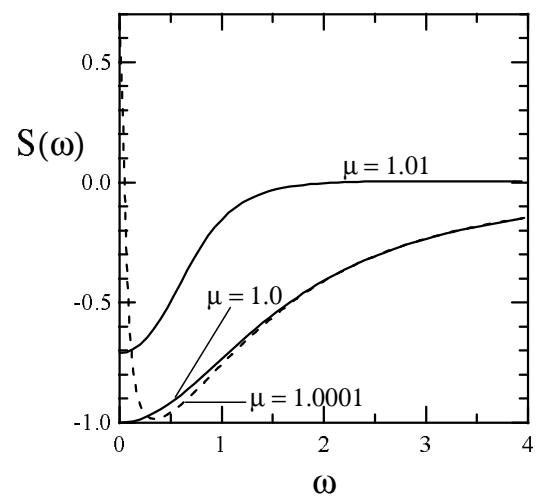


Pérez-Arjona et al.
 "Theory of quantum fluctuations..."
 Fig. 2

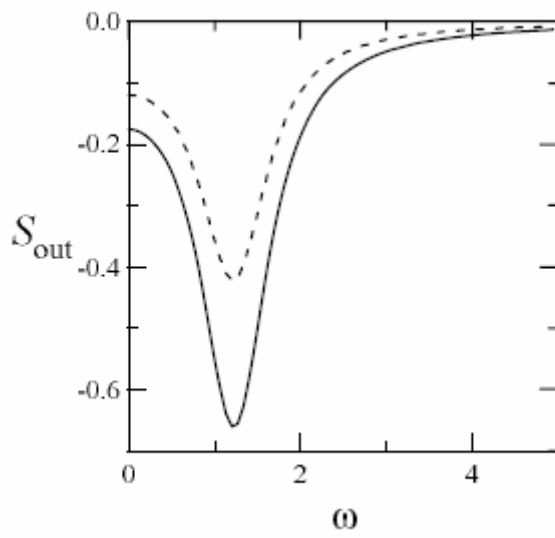
Perez-Arjona et al.
 "Theory of quantum fluctuations..."
 Fig. 3



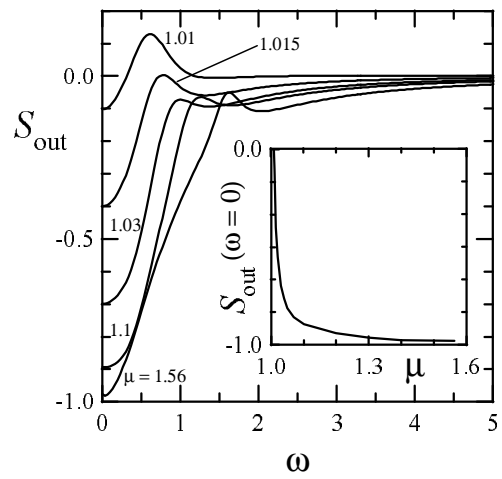
Pérez-Arjona et al.
"Theory of quantum fluctuations..."
Fig. 4



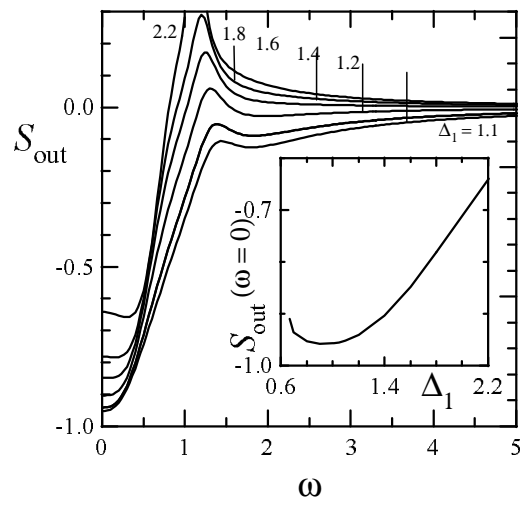
Pérez-Arjona et al.
"Theory of quantum fluctuations..."
Fig. 6



Pérez-Ajona et al.
 "Theory of quantum fluctuations..."
 Fig. 7



Pérez-Ajona et al.
 "Theory of quantum fluctuations..."
 Fig. 8



Pérez-Arjona et al.
"Theory of quantum fluctuations..."
Fig. 9

